



## Uncertainty impact on micro-vibration control of an orbiting large adaptive space structure

---

Federica Angeletti and Paolo Gasbarri

EasyChair preprints are intended for rapid dissemination of research results and are integrated with the rest of EasyChair.

November 19, 2018

# UNCERTAINTY IMPACT ON MICRO-VIBRATION CONTROL OF AN ORBITING LARGE ADAPTIVE SPACE STRUCTURE

Federica Angeletti\* and Paolo Gasbarri†

Large deployable structures are required for the advancement of modern space activities. A wide variety of EO (Earth Observation) satellites are actually using and will profit by large antenna systems supported by truss-like structures with low mass and stiffness. A net of smart actuators can be embedded in the supporting frame elements to make the structure adaptive itself and to limit undesired elastic vibrations. In the present paper, the supporting structure of a very large mesh reflector is investigated. An optimization procedure has been carried out to evaluate the damping efficacy of the actuators. After having assessed the best authority of the devices belonging to the active net, a control strategy has been implemented to coordinate their simultaneous action. One of the most relevant issues to ensure a good performance of a spacecraft integrated control strategy is related to its robustness when some uncertainty parameters are considered at design stage. In addition, the properties of space modules may be affected by slight changes due to launch loads. The effects of the attitude control authority and its robustness to uncertainties on mechanical and elastic parameters of both passive structure and actuators have been analysed and discussed.

## INTRODUCTION

The tendency of implementing large structures on spacecraft and narrowing performance requirements has significantly affected space activities lately. As for that, a consistent investigation aimed at coping with the interaction between platform control and flexible dynamics of the system is currently needed. The Control/Structure Interaction (CSI) can arise in various situations, thus entailing a deterioration of in-orbit performance that could be achieved by space systems. In-flight instability phenomena and even failure of the mission are undesired potential scenarios. Both latter and former have concerned telecommunication missions, with loss of operations time and achievable data.<sup>1</sup> Satellites equipped with wide lightweight flexible elements, as hoop reflector antennas, booms and long masts, call for the capacity of performing fast and precise manoeuvres without losing a strict control over flexible parts. Spacecraft equipped with large highly flexible appendages implies closely spaced structural modes and overlapping bandwidth.<sup>2</sup> Consequently, considering the CSI problem when designing satellites control systems is of paramount importance.

In recent years, advancements in counteracting CSI led to a significant increase of spacecraft reliability and operative life in modern space missions. Be it as it may, there exist a lack in alternative solutions other than classical suppression by feedback control system of the main rigid platform. The most widely used techniques are single loop frequency design methods, in particular a PID control for the rigid platform coupled with filters to eliminate resonant peaks of predominant elastic modes.<sup>3</sup> The shortage of available techniques stems mainly from scarcity of comprehensive understanding and implementation in the design phase

---

\* PhD Student, Mechanical and Aerospace Engineering Dept., Sapienza University of Rome, via Eudossiana 18.

† Associate Professor, Mechanical and Aerospace Engineering Dept., Sapienza University of Rome, via Eudossiana 18.

of the aforementioned interaction problem. It is therefore fundamental the design process is considered at an integrated system level.

Research has been conducted on active distributed control for large and highly flexible structures. This approach consists in stiffening the structure in an active control way by avoiding implementing more mass or material with higher Young modulus. Nevertheless, in the majority of current space missions, large antennas are supported by passive Extendable Supporting Structures (ESSs), thus unable to react to disturbances originated from platform operations and environmental perturbations. In a recent investigation conducted by Luo et al.<sup>4</sup>, the problem of active damping by piezo devices for hoop truss structures is addressed. Furthermore, a Fuzzy-based approach by Xu et al.<sup>5</sup> is implemented for a Gossamer space structure. On the contrary, according to the proposed approach, a network of smart piezoelectric devices can be embedded in the structure to make it adaptive.<sup>6</sup> In more detail, the attention has been focused on a specific kind of actuators, i.e. linear PZT stacks, where a small physical expansion along their length occurs when applying a voltage potential. This actuators category is currently available on the international market as devices to be used both in vacuum and extreme temperatures. In view of the above, in the paper a PD-feedback scheme with gains derived by a preliminary optimization procedure aimed at identify the devices authority is implemented and a robustness analysis (via Monte Carlo simulations) is performed to assess the efficacy of the strategy.

In this work, the mathematical model of an in-orbit spacecraft equipped with a mesh reflector supporting structure is reported. The equations of motion of the system are derived according to a classical Lagrangian formulation coupled with an alternative FEM formulation describing embedded piezo-actuators. Then, two optimization algorithms are implemented to find the set of gains that minimizes the power consumption of the control system. The method providing with the lowest sum of the gains is selected for further use. To conveniently implement a feedback control law based on the aforementioned gains, a state-space formulation is introduced. The main numerical results obtained after simulating a general spacecraft manoeuvre are reported and discussed. In the last section, the effects of uncertainties affecting piezo-devices and passive structures physical properties are investigated, as well as the impact of damaged actuators on the damping capabilities of the controller is considered and discussed.

## MATHEMATICAL MODELLING

The purpose of this paper is to investigate the ability of a network of piezo actuators to reduce the elastic vibrations induced on flexible appendices during an attitude manoeuvre, even if some parameters involved in the control laws are not known exactly. To this aim, a system configuration comprised of a central rigid satellite (1), a flexible boom (2) and a large antenna mesh structure (3) has been chosen to validate the active distributed control solution. The analysed antenna model is a planar structure composed of active truss elements, in a way to reproduce the reticular system that supports the reflector in the actual tri-dimensional case (see Figure 1).

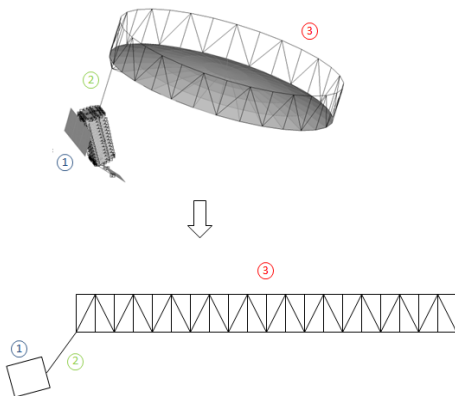


Figure 1. Planar system model

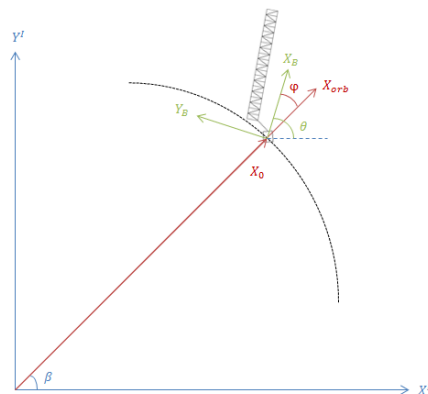


Figure 2. Reference frames

The spacecraft is hereby considered as a rigid hub equipped with a flexible appendage. The equations of motion of a flexible body in space environment are here presented according to a Lagrangian formulation complemented with FEM theory.<sup>7,8</sup>

## Kinematics

The motion of a generic point P of the body is given by the superposition of a rigid motion plus a set of structural modes.<sup>9</sup> As for that, the vector representing the position of the point P in an inertial, Earth-centred, reference frame is

$${}^I X_p = {}^I X_o + R \left( \xi + \sum_{k=1}^N A_k(t) \phi_k(\xi) \right) \quad (1)$$

$$R(\theta) = R_2(\beta) R_1(\varphi), \quad \theta = \beta + \varphi \quad (2)$$

where  ${}^I X_o$  represents the position vector of a generic body reference point in the inertial frame (selected as the platform centre of mass in this study),  $\xi$  is the aforementioned rigid motion associated at the point P in the body reference frame,  $\phi_k$  are the first N-set of the structure eigenvectors and  $A_k$  their relevant modal amplitudes. The matrix  $R$  describes the rotation from the body reference frame to the inertial one. This operation is accomplished in two steps. In the first place, we move from body reference frame to orbital axes by the means of the matrix  $R_1(\varphi)$  describing the attitude of the body with respect to the local vertical. Then, by using the matrix  $R_2(\beta)$  depending on the orbital parameter  $\beta$  (in-orbit position of the satellite), we arrive in the inertial frame. It is worth noting the terms in Equation (1) are of different orders of magnitude. The first one is of the order of the Earth equatorial radius, the second one of a characteristic dimension  $L$  of the body and the third one is the elastic deformation, a small fraction of  $L$ .

## Energy functionals

To write the equations of motion according to Hamilton's principle, the proper functionals have to be defined. The kinetic energy is defined as

$$K = \frac{1}{2} \int_B \dot{X}^T \dot{X} \mu dB \quad (3)$$

where  $\dot{X}$  is the derivative with respect to time of the position vector representing point P in the body reference frame. It can be expressed as

$$\dot{X} = T^{-1} {}^I \dot{X}_o + Ux + \dot{x} \quad (4)$$

with  $x$  position of the point, rigid plus elastic, in the body reference frame. The term  $U$  is an anti-symmetric matrix containing the angular velocity of the body.

For the potential energy we consider the elastic and piezoelectric contributions. For each finite element, the piezo materials constitutive equations can be written under the form<sup>8</sup>

$$\begin{aligned} T &= c^E S - e^T E_F \\ D &= e S + \varepsilon^S E_F \end{aligned} \quad (5)$$

where  $T$  is the stress vector,  $S$  the strain vector,  $E_F$  the electric field,  $D$  the electric displacement,  $c^E$  the elastic coefficient at constant electric field,  $e^T$  the piezoelectric coupling term and  $\varepsilon^S$  the dielectric coefficients at constant strain. According to linear piezoelectricity theory and IEEE88 standard, the electrical enthalpy  $H$  is defined as<sup>10</sup>

$$H = \frac{1}{2} [S^T T - E_F^T D] \quad (6)$$

the potential function can be written as

$$\Pi = \frac{1}{2} \int_B [S^T T - E_F^T D] \mu dB \quad (7)$$

By using the FEM approach, the displacement field  $X$  and the electric potentials  $\phi_i$  over the elements are related to the nodal values by the means of shape functions  $\Gamma$ , as described in the following relations:

$$\begin{aligned} x &= \Gamma_X x_i \\ \phi &= \Gamma_\phi \phi_i \end{aligned} \quad (8)$$

Therefore, the strain field and the electric field are related to nodal values by shape functions derivatives  $B$

$$\begin{aligned} S &= D \Gamma_X x_i = B_X x_i \\ E_F &= -\nabla \Gamma_\phi \phi_i = -B_\phi \phi_i \end{aligned} \quad (9)$$

where  $D$  is a matrix containing differential operators. Considering Equations (7)-(9), the potential energy becomes

$$\Pi = \frac{1}{2} x^T K_{XX} x + x^T K_{X\phi} \phi - \phi^T K_{\phi\phi} \phi \quad (10)$$

$$K_{X\phi} = \int_B B_X^T e^E B_\phi \mu dB; \quad K_{X\phi} = \int_B B_X^T e^E B_\phi \mu dB; \quad K_{\phi\phi} = \int_B B_\phi^T \varepsilon^S B_\phi \mu dB \quad (11)$$

The gravitational potential can be defined as a Newtonian potential acting on a point at distance  $r$  from the Earth center. The expression is presented below

$$V = -\frac{\mu}{r} = -\mu_o \int_B \rho \frac{1}{\sqrt{X^T(x) X(x)}} dB \quad (12)$$

where  $\mu_o$  is the Earth's gravitational constant.

## FEM formulation

The antenna structure is composed of ten modules (or bays) with the same geometrical and physical properties. To study the dynamic behaviour of the flexible appendix, the FEM approach is needed (see Figure 3). The structural components are modelled as beams with three degrees of freedom for each node as indicated in Figure 5. Each truss is further divided into three elements to enhance the finite elements representation of the system dynamics. The boom is made up of eight beams elements, with different geometric and physics properties with respect to the antenna ones. The system comprises 251 elements connected by 212 nodes, reaching a total of 636 degrees of freedom.

The local stiffness and mass matrices of the two-node passive beam are implemented according to classical FEM theory. The local matrices are then assembled in global ones by using a mapping matrix describing the interconnections and orientation of nodes and trusses in the plane. The complete stiffness and mass matrices, as well as the eigenvalue and modes originated from the assembled system, have been computed by the means of a MATLAB FEM code and then validated by comparison with a commercial software (i.e. MSC Nastran).

To effectively counteract undesired elastic vibrations on both boom and antenna structures, a set of piezo-electric devices has been embedded within the beams. The mass associated to the active devices is not neglected in this study. The device action is meant to be applied only to the axial beam direction, due to the reticular nature of the structure. It is possible to determine the equivalent stiffness parameter to be used in the finite element formulation.<sup>11</sup> We can imagine segmenting the adaptive-truss in three parts: a central active and two symmetrical passive parts. The parts are considered as rigidly connected between them. The

central part length is equal to the dimension of the piezo-devices, while the lateral ones can vary accordingly to the selected structure. In this case, they have equal lengths. Concerning the central active part, an equivalent stiffness coefficient can be defined by considering the stiffness of the host structure in parallel with the stiffness of the active device embedded in it.

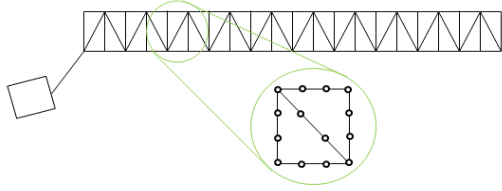


Figure 3. FEM discretization



Figure 5. Passive beam element

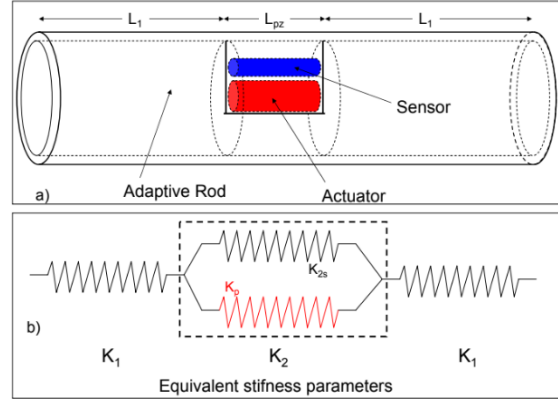


Figure 4. Equivalent stiffness formulation

Referring to Figure 4, we can write

$$K_1 = \frac{EA}{L_1} \quad (13)$$

$$K_2 = K_{2a} + K_{pz} = \frac{E(A - A_{pz})}{L_{pz}} + \frac{E_{pz}A_{pz}}{L_{pz}} \quad (14)$$

The equivalent stiffness parameter for the whole element is finally defined as the series of three “elastic springs”

$$K_{eq} = \frac{K_1 K_2}{2K_2 + K_1} \quad (15)$$

### Equilibrium equations

The equations of motion can be derived according to a classical Lagrangian approach. By referring to  $L$  as the Lagrangian

$$L = K - \Pi - V \quad (16)$$

the equations can be written in the form

$$\frac{d}{dt} \frac{\partial L}{\partial \dot{S}} - \frac{\partial L}{\partial S} = F_L \quad (17)$$

with the generalized forces acting on the system (other than the gravitational ones, as the control forces).

By performing the relevant algebra, not reported here for the sake of brevity, it is possible to obtain the non-linear dynamics of a flexible spacecraft under the gravity and gravity gradient field effects when the structural elements contain piezoelectric stacks actuators. The equations of motion are hereby reported:

$$M\ddot{X}_O + \omega \wedge (\omega \wedge \tilde{p}) + 2\omega \wedge \sum_{k=1}^N \gamma_{T_k} \dot{A}_k + \dot{\omega} \wedge \tilde{p} + \sum_{k=1}^N \gamma_{T_k} \ddot{A}_k = F_G + F_C \quad (18)$$

$$\tilde{p} \wedge \dot{X}_O + J \ddot{\omega} + \sum_{k=1}^N \sum_{l=1}^N \Upsilon^{kl} \dot{A}_l \dot{A}_k + \sum_{k=1}^N \gamma_{R_k} \ddot{A}_k + \omega \wedge \sum_{k=1}^N \gamma_{R_k} \dot{A}_k = C_G + \tau_C \quad (19)$$

$$\gamma_{T,k}^T \ddot{X}_O + \gamma_R^T \dot{\omega} + \ddot{A}_k + \Omega_k^2 A_k + 2\xi_k \Omega_k \dot{A}_k + 2\omega^T \sum_{l=1}^N \Upsilon^{kl} \dot{A}_l + \tilde{K}_{X\phi,k} \phi_k = \tilde{F}_{G,k} \quad (20)$$

$$\tilde{K}_{X\phi,k}^T A_k - K_{\phi\phi,k} \phi_k = Q_k \quad (21)$$

where  $M$  is the total mass of the system,  $\omega$  indicates the angular velocity of the spacecraft,  $J$  is the rotational inertia of the system,  $\Omega_k$  represents the  $k$ -th eigenfrequency of the structure,  $\xi_k$  is the damping coefficient and  $Q$  is the electric displacement vector. The control forces applied to the platform are referred as  $F_C$  and  $\tau_C$ . It is worth noting the static moment  $p$  derives from the choice of the body reference frame origin as the centre of mass of the platform without the flexible appendage. Furthermore, the static moment depends also on the elastic displacements through the modal participation factors  $\gamma_{T_k}$  and the modal amplitudes. Indeed, we can write

$$\tilde{p} = p + \sum_{k=1}^N \gamma_{T_k} A_k \quad \text{with} \quad p = \int_B \xi \rho dB \quad (22)$$

where the modal participation factors are

$$\begin{aligned} \gamma_{T_k} &= \int_B \rho \phi_k dB \\ \gamma_{R_k} &= \int_B \xi \wedge \phi_k \rho dB \\ \gamma_{kl} &= \int_B \phi_k \wedge \phi_l \rho dB \end{aligned} \quad (23)$$

Due to the large number of the finite element model DOFs, a truncated modal matrix including only the first  $h$  modes (normalized with respect to mass) has been introduced to reduce the system variables and avoid an exceedingly high computational cost. The nodal displacement vector can be written in the modal domain as

$$x = \phi_s A \quad (24)$$

As a consequence, after having left-multiplied the third equation of motion by the transposed modal matrix the electro-mechanical coupling matrix becomes

$$\tilde{K}_{X\phi} = \phi^T K_{X\phi} \quad (25)$$

The gravitational terms are listed below

$$\begin{aligned} F_G &= -M \mu \frac{\hat{s}}{|X_0|^2} \quad \text{with} \quad \hat{s} = \frac{X_0}{|X_0|} \\ C_G &= -\frac{\mu \hat{s}}{|X_0|^2} (\tilde{p} \wedge \hat{s}) + \frac{3\mu J}{|X_0|^3} \cos \varphi \sin \varphi \\ \tilde{F}_{G,k} &= -\frac{\mu}{|X_0|^2} (\hat{s}^T \gamma_{T,k}) \end{aligned} \quad (26)$$

where  $F_G$  is the vector of gravitational forces in the Inertial Reference frame,  $C_G$  indicates the gravity gradient torque in the Body Reference frame and  $\tilde{F}_{G,k}$  is the generalized gravitational force projected on the  $k$ -th elastic mode. The term  $\hat{s}$  is the versor of the local vertical passing through the origin of the Body Reference Frame.

## OPTIMIZATION PROCESS

To better understand the effect of purely active damping on the structure the flexible structure has been initially studied blocking the satellite's degrees of freedom, i.e. in a cantilever configuration. On account of this the rigid motion of the spacecraft is avoided and the relevant dynamic equations reduce to the ones of its flexible parts that are modelled via FEM approach through the mass, the stiffness and the damping matrices. Considering the piezo actuators effect as a direct velocity feedback, their contribution to the system dynamics can be schematized considering an additional damping  $C_{pz}$  in the FEM modelling:

$$M\ddot{X} + (C_S + C_{pz})\dot{X} + KX = F \quad (27)$$

where  $C_S = \alpha M + \beta K$  models the structure passive damping. It is demonstrated [26] the active damping matrix can be formulated for each element as

$$C_{pz,k} = g_k 2 \frac{E_{pz} A_{pz} G}{L_{pz} \delta_{pz}} \begin{bmatrix} 1 & -1 \\ -1 & 1 \end{bmatrix} \quad (28)$$

where  $g_k$  is the gain of the k-th element (and it is associated to the power consumption necessary to introduce an active damping in the adaptive-truss),  $G$  is a coefficient dependent on the piezo-device physics properties (Young module, area, length, electrical resistance, electromechanical coupling coefficient),  $\delta_{pz}$  is a non-dimensional parameter referring to the piezo-electric device length. The global matrix can be obtained by following the conventional FEM assembling methods. The model here investigated is the one reported in Figure 3. Each structural part has a length of 1 meter. The spacecraft appendage is composed of a deployed boom and the antenna supporting truss structure. Their physical and geometrical properties are listed in Table 1. The boom and the antenna frame are realized in composite material, with different section areas. The main mechanical properties are presented in Table 2.

**Table 1. Properties of the system**

	Platform	Boom	Antenna
Length (m)	2	4	20
Mass (kg)	500	152.3	57.95
Inertia (kg m <sup>2</sup> )	333.3	1.464e4	
F.E.	/	8	243

**Table 2. FEM mechanical properties**

	Boom	Antenna
Area (m <sup>2</sup> )	0.0236	3.92e-4
Young Modulus (GPa)	150	200
Density (kg/m <sup>3</sup> )	1800	1700

A modal analysis has been performed to assess the first frequencies and modal shapes of the appendage in the case the boom is clamped at its end. The first five frequencies are reported in Table 3. For convenience's sake, the corresponding modal shapes obtained by using the Matlab FEM code are presented too. By projecting the equations of motion on a modal basis, the damping coefficient  $\xi = 0.02$  has been added. The eigenvalues observed in the case of structural damping are reported in complex conjugated couples as well.


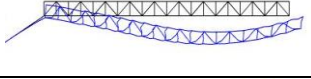
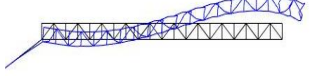

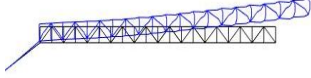
In the following sections, two methods to actively control the first five modes of the structure are introduced and their results presented.

### Optimization procedure A: Genetic Algorithm

The pole placement procedure aims at individuating the minimum gain distribution such that the real parts of a selected number of eigenvalues from the homogeneous eq. (43) have an assigned value higher than the respective eigenvalues originated by the presence of the solely passive structural damping.



**Table 3. Frequencies of the clamped appendage**

N°	Frequency (Hz)	Modal Shape	Eigenvalues
1	1.92		$-0.24 \pm 12.09i$
2	9.80		$-1.23 \pm 61.59i$
3	20.26		$-2.55 \pm 127.27i$
4	43.04		$-5.41 \pm 270.42i$
5	51.11		$-6.52 \pm 326.10i$

The problem may be formulated as a constrained optimization problem in the following terms:

*Find the gains vector  $g$  to minimize the function  $\Lambda(g)$  subjected to the constraints  $\lambda_i \geq \lambda_i^*$ ,  
with  $(i = 1, \dots, N_c)$  and  $g_l \leq g_k \leq g_u$*

where  $N_c$  is the number of constraints,  $\Lambda(g)$  is the objective function defined as

$$\Lambda(g) = \sum_{k=1}^{N_a} g_k \quad (29)$$

$N_a$  is the number of active trusses and  $\lambda_i^*$  the assigned constrained value on the real part of the eigenvalue  $\mu(g)$  obtained from the equations

$$|A - \mu(g)B| = 0 \quad (30)$$

$$A = \begin{bmatrix} 0 & -I \\ K & C(g) \end{bmatrix} \quad B = -\begin{bmatrix} I & 0 \\ 0 & M \end{bmatrix} \quad U = \begin{bmatrix} X \\ \dot{X} \end{bmatrix} \quad (31)$$

where the generic eigenvalue is defined by

$$\mu = -\lambda \pm j\delta \quad (32)$$

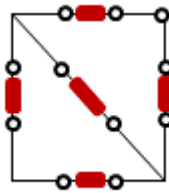
In this case study, the first five modes are simultaneously controlled. The imposed constraints guarantee an increase on the real part of the controlled eigenvalue greater than 10% of the respective passive structure, i.e.

$$\lambda_i > (1 + 0.1)\lambda_{0i} = \lambda_i^*, \quad i = 1, \dots, 5 \quad (33)$$

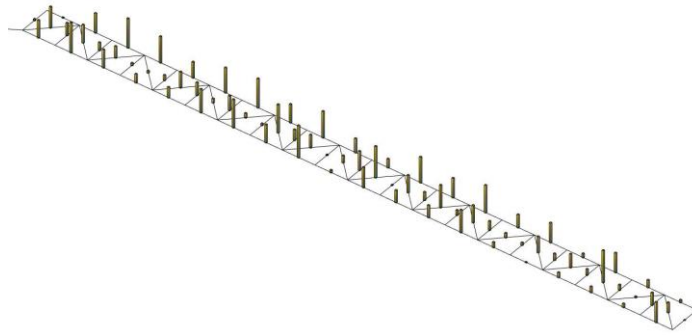
The optimization algorithm is here performed through a Genetic Algorithm (GA) technique based on Augmented Lagrangian Genetic Algorithm (ALGA), in order to solve the optimization problem subjected to non-linear constraints.

In this case, the project variables to be determined are 251, one gain for each potentially active element of the entire structure. Due to the great amount of variables and to the excessive computational time, a trade-off choice has been validated: the piezo-electric devices are solely activated (i.e. their gain is greater than zero) if they exist in the middle elements of each bay (as highlighted in red in Figure 6). According to

this approach, the parameters to be optimized reduce to 81 variables. The algorithm converged to an optimal solution in the gains range [0-50]. The gain distribution histogram plot is presented in Figure 7.



**Figure 6. Position of active devices**



**Figure 7. Gains distribution histogram**

A good enhancement of the damping properties of the system can be observed, due to the piezo-electric devices contribution. The new values of the first five structural eigenvalues are listed in Table 4. After having obtained the best authority of the adaptive trusses thanks to the optimization process, the structure dynamic behaviour when perturbed with some external forces has been investigated.

**Table 4. Active damping: Genetic algorithm**

N°	Eigenvalues
1-2	$-0.31 \pm 12.09i$
3-4	$-3.06 \pm 62.02i$
5-6	$-9.11 \pm 130.27i$
7-8	$-19.35 \pm 287.42i$
9-10	$-23.12 \pm 358.10i$

The total sum  $\Lambda(g)$  of the network gains can be assumed as a quality parameter giving information about the power consumption: the less the sum, the less the power consumption. In the present analysis, the total sum is equal to 1703.5.

### Optimization procedure B: Reinforcement Learning Algorithm

An alternative method to find an optimal distribution of derivative gains is to adopt a Reinforcement Learning (RL) algorithm. Roughly speaking, the RL agent wants to learn how to select the controller gains in order to maximize a given reward signal.<sup>12</sup> The aim here is to estimate an action-value function and consequently to optimize a policy  $Q(s,a)$ , i.e. to estimate the best decisional policy  $Q^*(s,a)$  for a set of states  $s$  and actions  $a$  by improving the initial one until the condition  $Q(s,a) \sim Q^*(s,a)$  is achieved. This leads to a mapping of the actions (i.e. the gains) the agent can select to optimally control the first five modes of the flexible system, according to its initial state.

The choice of states and actions is of paramount importance for a successful RL method. According to the objective of this paper, the actions are chosen as the actuators gains itself. The agent can decide if assign to the net of active device an equally spaced finite value included in the interval [0-50]. The states variables are referred to the real part of the eigenvalues with respect to the desired increased value  $\lambda_i^*$ . Indeed, the state variables are five, one for each mode to be controlled. They can assume a single value between the numbers [-0.5, 0, 0.5], respectively if the real part of the eigenvalue is lower, equal or higher than the corresponding  $\lambda_i^*$ . This leads to a total amount of  $3^5$  possible states combination. If considering 51 possible ac-

tions values, each Q-table will be composed of 243 rows and 51 columns, for a total of 81 Q-tables of 12393 elements each (i.e. one Q-table per actuator).

The reward function is needed to define the desired goal in the RL problem. This operation associates a combination of state-action with a numerical signal which indicated the “goodness” of that state-action pair. In this perspective, the RL agent search to maximize the absolute value of the real part of the first five eigenvalues to reduce undesired vibrations. Since the goal of the agent is to increase the damping capability of the structure while maintaining minimum the sum of the gains, the reward signal is here defined as:

$$R_s = (\delta d_1^2 + d_2) \quad \text{with} \quad (34)$$

$$d_1 = \sum_{i=1}^5 \chi_i |\lambda_i - \lambda_i^*| \quad d_2 = \frac{1}{\text{sum}(g)}$$

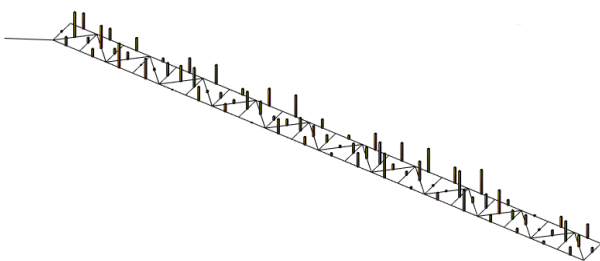
where  $\delta$  is a scaling coefficient introduced to match the orders of magnitude of the two rewarding terms. The variable  $\chi_i$  is a weighting coefficient different for each eigenvalue, here adopted to give more emphasis to the damping of the first fundamental frequency in the perspective of CSI issue mitigation.

The adopted algorithm is named SARSA (State Action Reward State Action), whose updating rule involves the current state and action and the reward corresponding to the transition into the next state by selecting one of the next available actions. In particular, the change to the policy after an agent’s interaction with the environment influence future decisions. At the end of the procedure, we can obtain a set of gains to be implemented in the control scheme. The relevant gain distribution histogram is reported in Figure 8. The new values of system eigenvalues are reported in Table 5. We can notice the first ones are in agreement with those individuated by using the GA algorithm.

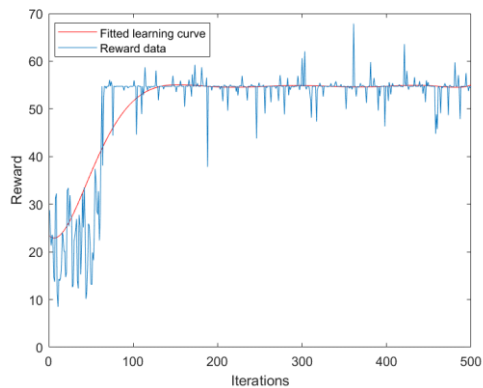
**Table 5. Active damping: RL algorithm**

N°	Eigenvalues
1-2	-0.32 ± 12.09i
3-4	-3.20 ± 61.98i
5-6	-8.89 ± 129.87i
7-8	-19.66 ± 286.43i
9-10	-21.13 ± 357.20i

In particular, Figure 9 depicts the progression of the reward signal through iterations. The convergence of the learning process is reached after few iterations and the fitted learning curve is reported in red.



**Figure 8. Gains distribution histogram**



**Figure 9. Learning curve**

The total sum of the gains is equal to 1782.3. In this case, we can notice a good enhancement of the damping properties of the system with slightly higher gains than the previous case.

## INTEGRATED CONTROL SYSTEM

As stated before, the interaction between satellite motion and flexible vibrations can heavily disturb the stability of the system. Many control strategies have been developed for solving this issue. Some of them are focused on the attitude dynamics, building on robust controllers that consider flexibility as a disturbance, as well as on model-based controllers in which an effort is done to include a dynamic model both for the rigid and the elastic dynamics. The objective of this paper is to study a different approach, consisting in facing the problem from the structural point of view, trying to actively damp the vibrations induced by the attitude control system and the orbital perturbations, by using smart material stack devices. As for that, the objective results in simultaneously optimizing the controller gains and the damping of the flexible modes, to avoid coupling between the control system and the satellite flexible structure dynamics. The gains derived from the RL optimization procedure are further used to validate the control for a typical spacecraft manoeuvre.

To solve the problem of the spacecraft dynamics, the system of equations (18)-(21) have been recast as a set of first order differential equations, written in the state-space form, to be easily implemented and computed by using MATLAB/Simulink environment. By defining the state vector  $X$ , the electric displacement output vector  $y$  and the control input  $u$  as

$$X = \begin{bmatrix} X_0 \\ \theta \\ A \\ \dot{X}_0 \\ \dot{\theta} \\ \dot{A} \end{bmatrix} \quad y = Q_s \quad u = \phi_a \quad (35)$$

the equations can be re-arranged in the state-vector space as

$$\begin{cases} \dot{X} = AX + Bu + g \\ y = CX + Du \end{cases} \quad (36)$$

$$A = \begin{bmatrix} 0 & 0 & 0 & I_2 & 0 & 0 \\ 0 & 0 & 0 & 0 & 1 & 0 \\ 0 & 0 & 0 & 0 & 0 & I_h \\ M^{-1}K & & & M^{-1}C & & \end{bmatrix} \quad B = \begin{bmatrix} 0 \\ M^{-1}\tilde{K}_{X\phi} \end{bmatrix} \quad C = [0 \quad \tilde{K}_{X\phi}^T \quad 0] \quad D = K_{\phi\phi} + D_{RM} \quad (37)$$

$$g = \begin{bmatrix} 0 \\ N_L + F_G^g + F_C^g \end{bmatrix} \quad (38)$$

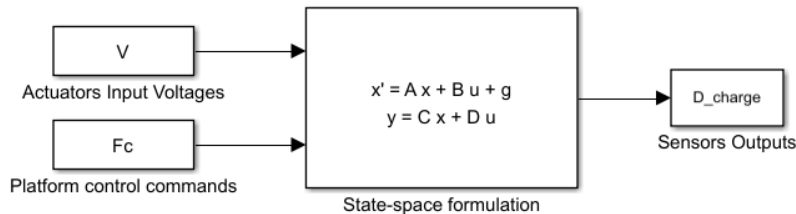
where  $N_L$  indicates the non-linear terms,  $F_G^g$  is the vector of the aforementioned generalized gravitational forces and  $F_C^g$  the generalized control forces acting on the spacecraft. Furthermore, the following notation had been adopted

$$M = \begin{bmatrix} m & \tilde{p} & \gamma_T \\ \tilde{p}^T & J & \gamma_R \\ \gamma_T^T & \gamma_R^T & I \end{bmatrix} \quad K = \begin{bmatrix} 0 & 0 & 0 \\ 0 & 0 & 0 \\ 0 & 0 & \Omega^2 \end{bmatrix} \quad C = \begin{bmatrix} 0 & 0 & 0 \\ 0 & 0 & 0 \\ 0 & 0 & 2\xi\Omega \end{bmatrix} \quad (39)$$

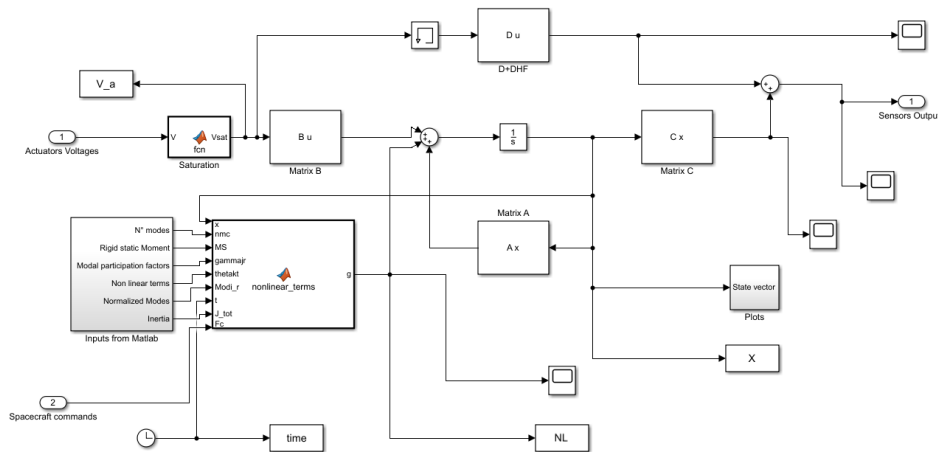
The matrix  $D_{RM}$  is introduced here to take into account the contribution of the modes outside the bandwidth. The term is often called ‘‘residual modes’’ and the formulation is presented below <sup>8,10</sup>

$$D_{RM} = -(K_{X\phi}^T K_{XX}^{-1} K_{X\phi}) - \sum_{k=1}^N \frac{(K_{X\phi}^T \phi_s)(\phi_s^T K_{X\phi})}{\Omega_k^2} \quad (40)$$

In particular, the model has been implemented in MATLAB/Simulink environment to simulate the behaviour of the dynamic system (see). The general model accepts as inputs the voltages required by the piezo actuators to damp the elastic vibrations induced on the antenna by the platform control commands. To actively damp elastic vibration induced in flexible structures smart devices can be used both as actuators and sensors. A control strategy has been implemented to control the elastic vibrations induced on the antenna supporting structures due to a spacecraft re-orienting manoeuvre. Furthermore, the control inputs are processed by a saturation block before being assigned to each smart actuator, thus ensuring the piezoelectric materials operates in a safety state.



**Figure 10. General state-space formulation**



**Figure 11. Dynamic system scheme (State-space formulation block of Figure 10)**

A PD strategy can be applied to actively control the vibrations of the appendage. The actuation voltages are

$$\phi_a = \alpha A + \beta \dot{A} \quad (41)$$

By comparing Equation (27) and Equation (20) the gains for the PD control law can be established as

$$C_{pz} \phi_h = K_{X\phi} \beta \rightarrow \beta = K_{X\phi}^+ (C_{pz}(g) \phi_h) \quad (42)$$

where  $K_{X\phi}^+$  represents the Moore-Penrose inverse of the electro-mechanical coupling matrix. The coefficient  $\alpha$  is introduced to simultaneously act on the stiffness of the system. According to this approach, the results coming from the optimization procedure can be directly inserted in the control scheme.

## NUMERICAL RESULTS

The control strategy has been applied to the case of an orbiting spacecraft to analyse its effectiveness. The system consists of a main platform and a flexible appendage. The properties of the whole system are presented in Table 1. The truss-like frame is equipped with smart actuators whose properties are listed in Table 6. To consider a real case, the chosen orbit is similar to the one adopted for the SMAP mission, which is currently equipping a mesh reflector. The chosen parameters are presented in Table 7.

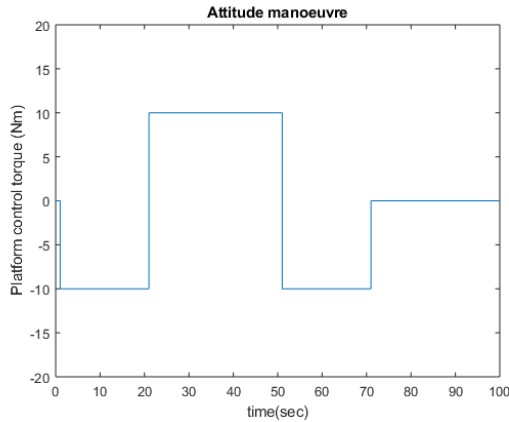
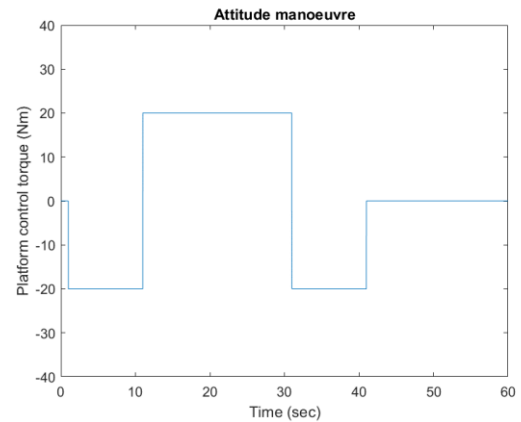
**Table 6. Smart devices physical properties**

	Smart device
Area (m <sup>2</sup> )	5.92e-5
Young Modulus (GPa)	130
Density (kg/m <sup>3</sup> )	7000
Electro-mechanical coupling coefficient $d_{33}$ (V/m)	400e-12
Resistance, R (Ohm)	2000
Electric capacitance $C_p$ ( $\mu$ F)	33
Max/Min Voltage (V)	$\pm 140$

**Table 7. Orbital parameters**

	Symbol	Value
Eccentricity	e	0
Orbital radius	R	7078 km
Initial position on the orbit (angle)	$\beta$	25 deg
Initial orientation w.r.t. the local vertical	$\varphi$	5 deg
Orbital period	$T_o$	98.77 min

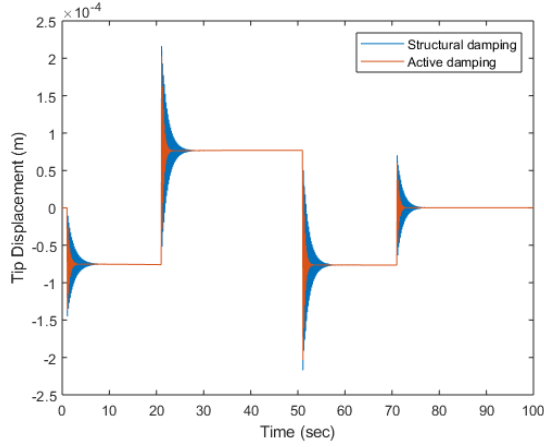
Two attitude manoeuvres have been simulated to study the influence of the control on the antenna elastic displacements. Two simple bang-bang manoeuvres are reported in Figure 12 and Figure 13. Manoeuvre A aims at reproducing a possible attitude modifying operation, by using only a platform control torque. On the contrary, the other option represents a faster manoeuvre, thus demanding a higher control effort.

**Figure 12. Attitude manoeuvre A****Figure 13. Attitude manoeuvre B**

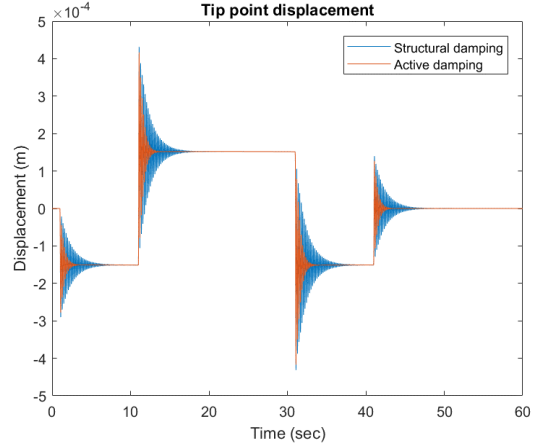
The resulting displacements at the tip of the antenna are presented in Figure 14 and Figure 15. The active network is able to effectively damp the unwanted elastic vibrations in few seconds. Then, the time histories related to actuator N°9 input voltages are reported in Figure 16 and Figure 17. A factor of safety was introduced to the control scheme to additionally lower the maximum allowable input signal and enhance the reliability of the system.

According to this approach, the voltage level corresponding to the physical limit of piezoelectric devices is not reached by the control system. It is worth noting the actuators with a higher derivative gain (corresponding to the one obtained from the optimization procedure) reach the saturation condition (as in Figure 17). As for that, the control channel is saturated for a few seconds, but this event still does not compromise the effective damping capability of the active system.

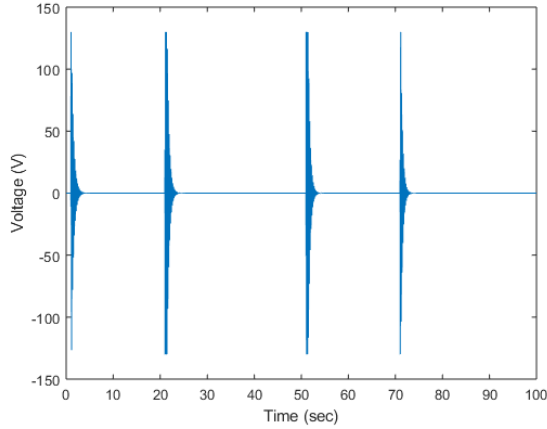
All things considered, manoeuvre B has been selected for further analyses as it leads to a larger maximum tip displacement and the aim of the paper is to validate the control strategy assuming the worst operating conditions.



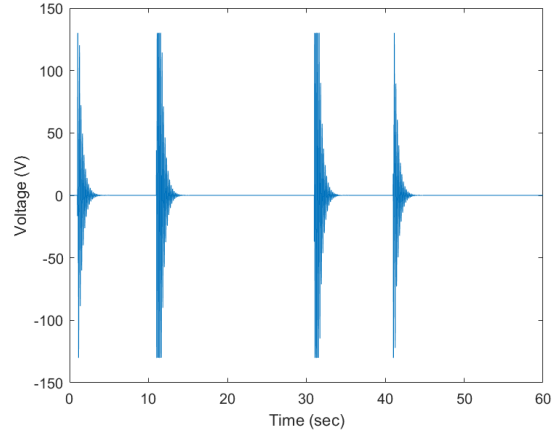
**Figure 14. Manoeuvre A: Tip displacement**



**Figure 15. Manoeuvre B: Tip displacement**



**Figure 16. Manoeuvre A: Input voltage time history (actuator N° 9)**



**Figure 17. Manoeuvre B: Input voltage time history (actuator N° 9)**

To evaluate the power consumption required by the active devices network, the mean power absorbed by each actuator has been computed as

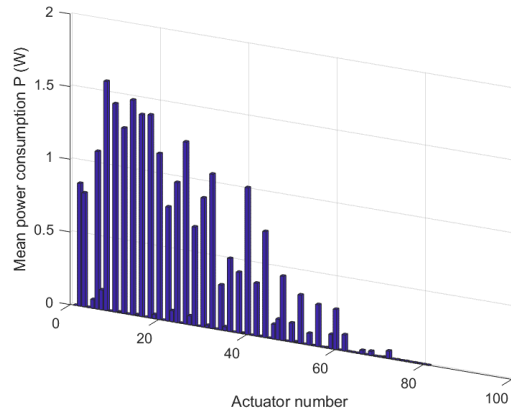
$$\bar{P}_i = \frac{1}{T_F} \int_0^T P_i(t) dt = \frac{1}{T_F} \int_0^T C_p V_i^2(t) dt \quad (43)$$

where the  $i$ -index indicates the actuator number,  $T_F$  is the total manoeuvre time,  $C_p$  the electrical capacitance (as reported in Table 6) and  $V_i$  the voltage supplied to each device. The average power consumption  $\bar{P}_i$ , referred to each actuator, is showed in Figure 18.

It can be noticed the actuators requiring most of the power are those placed near the boom. This result is expected if considering that the antenna frame structure receives the perturbation originated by the satellite motion through the boom itself.

The total mean power consumption is computed as

$$\bar{P} = \sum_{i=1}^{81} \bar{P}_i = 23.97 \text{ W} \quad (44)$$



**Figure 18. Mean power consumption per actuator**

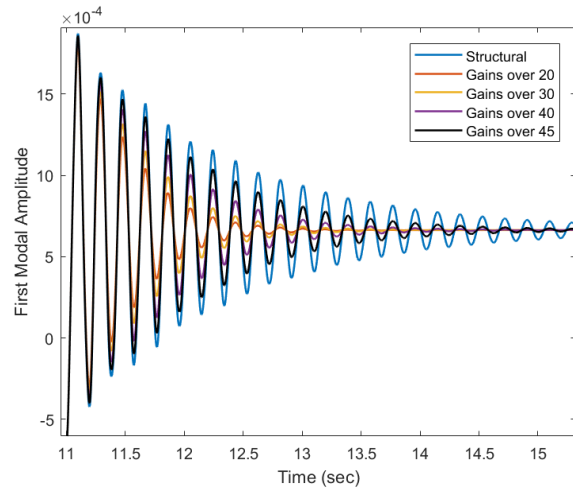
According to the available data about SMAP (Soil Moisture Active Passive) spacecraft accoutred with the patented Astromesh reflector, its solar panels can generate 1500 Watts of electric power. As for that, the power amount reserved to the active damping system seems to be bearable for the mission.

### LIMITED NUMBER OF ACTUATORS

A further analysis has been performed to assess what happens if the control system switches off some actuators associated to gains under a specific threshold. By way of explanation, two operative modes have been assigned to the smart devices: ON and OFF. Once identified a threshold  $T_G$  in the range [0-50], if the piezoelectric element is actuated with a gain whose value is over  $T_G$  its mode will be ON. It will be then operated by using the unmodified gain value, otherwise its mode will be OFF (i.e. gain equal to zero). The number of ON-mode devices and the required total average power are listed in Table 8.

**Table 8. Different thresholds**

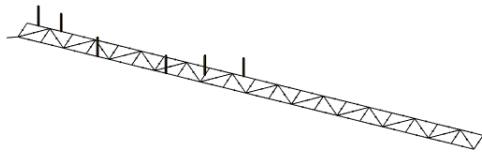
Threshold	N° of ON actuators	N° of OFF actuators	Average Power (W)
$T_G = 20$	40	41	16.03
$T_G = 30$	21	60	12.25
$T_G = 40$	12	69	8.66
$T_G = 45$	6	75	5.02



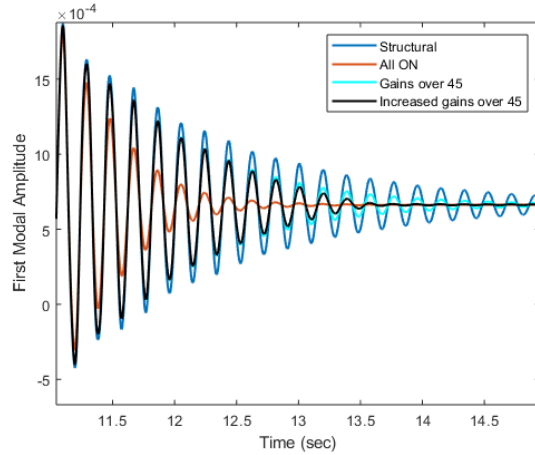
**Figure 19. First modal amplitude**

It can be noticed the damping capability of the system decreases when reducing the number of active devices. In parallel, the absorbed power diminishes as the gains remain the same. The ON-actuators left when considering  $T_G = 45$  are showed in Figure 20.





**Figure 20. Gains over  $T_G = 45$**



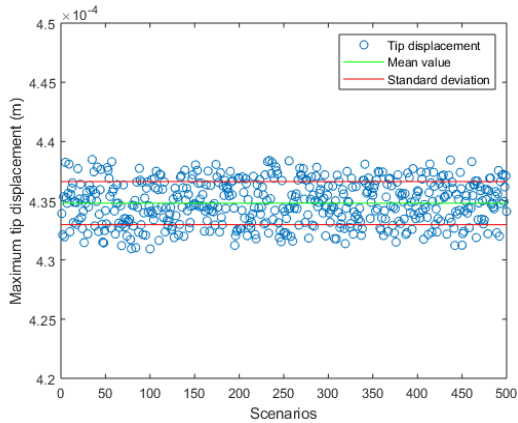
**Figure 21. Effects of increasing gains over  $T_G = 45$**

If the gains of the six actuators are increased by a factor  $10^3$ , no significant improvement in damping the vibration amplitude is noticed as depicted in Figure 21, even if the total power consumption reaches 72 Watts. We can deduce that by using all the optimized gains the system is able to cope with elastic vibrations better than by having some of them switched off, allowing a lower power consumption in addition.

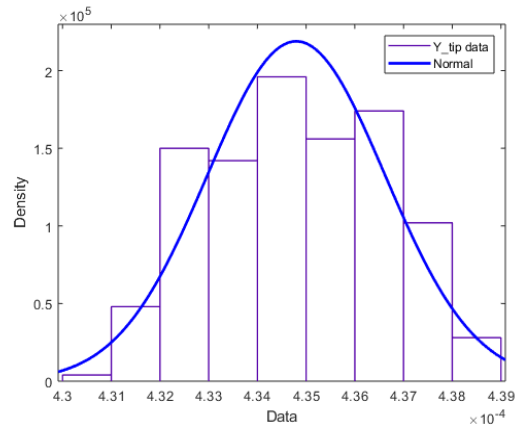
## DAMAGED ACTUATORS

In this section, another aspect will be analysed: the robustness of the actuators network in damping the vibration when one or more devices are in a “damaged” condition. The decrease of the piezoelectric physical and electromechanical properties is modelled as a gain reduction of the 50% on randomly chosen actuators. In particular, a number  $N$  of randomly selected devices has been considered as damaged and a Monte Carlo simulations campaign has been carried out to verify the impact of properties decrease on the controller efficacy.

A first analysis has been performed by fixing  $N=40$ . More thoroughly, five-hundred simulations has been repeated to study the change in the network damping behaviour. The data concerning the maximum tip displacement gathered via simulations are depicted in Figure 22. A Normal fit distribution has been evaluated starting from data density, as indicated in Figure 23.



**Figure 22. Maximum tip displacement:  $N=40$ ,  $\mu = 4.3480e-04$ ,  $\sigma = 1.8222e-06$**



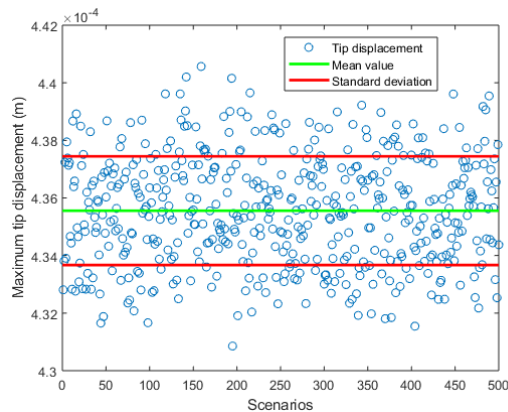
**Figure 23. Normal distribution of tip displacement data set**

The change in the tip displacement maximum value has been analysed. The collected data have been processed by the means of the MATLAB Distribution Fitting Toolbox. Their mean value  $\mu$  and standard deviation  $\sigma$  have been computed as

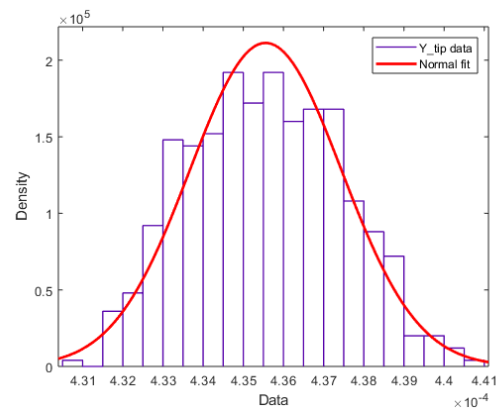
$$\mu = \frac{1}{N} \sum_{i=1}^N Y_{TIP_i} \quad \sigma = \sqrt{\frac{1}{N-1} \sum_{i=1}^N |Y_{TIP_i} - \mu|^2} \quad (45)$$

According to the results, no significant impact has been detected on the controller, since the maximum tip displacement is not increasing if some actuators are damaged.

To enhance the reliability of the control scheme, a random number  $N$  between the half and the total number of the actuators has been considered as damaged during the manoeuvre simulation. In order to have a representative set of results, 500 scenarios were considered. To make a comparison with the previous case study, both the trend of maximum tip displacements and the data normal fit are presented in Figure 24 and Figure 25.



**Figure 24. Maximum tip displacement:**  $N$  random,  $\mu = 4.3556e-04$ ,  $\sigma = 1.8880e-06$



**Figure 25. Normal distribution of tip displacement data set**

It is worth noting that, according to simulations, also in this case the system proves to not be significantly influenced by the damages of piezo-electric devices. No heavy differences between the two cases are identified, thus meaning that even if the number of imperfect actuators overcomes the half of the total the active network is still able to counteract the undesired elastic oscillations.

## ROBUSTNESS ANALYSIS

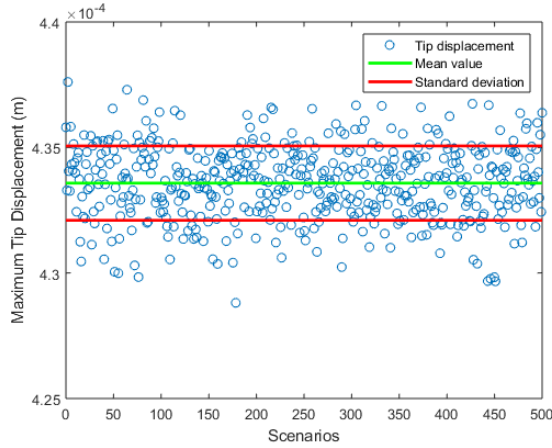
The verification of the control performance is based on a Monte Carlo campaign. This method has been selected as it allows to study the behaviour of a simulated system under different conditions. Four case studies, as described in Table 9, have been investigated. The properties of both active network devices and passive supporting structure are assumed as uncertain to simulate a possible change in the mechanical and electrical characteristics after launch or due to in-orbit aging.

Affected features are:

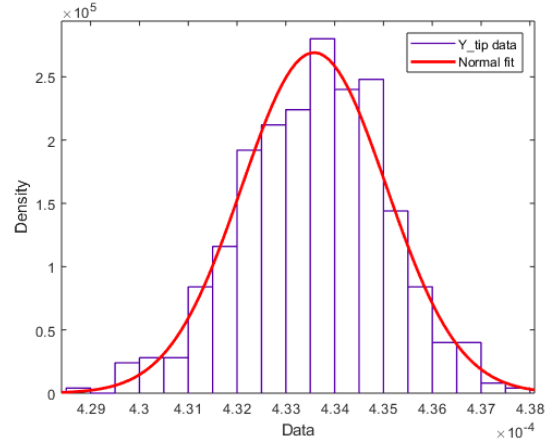
- Piezo devices: length  $L_{pz}$ , Young modulus  $E_{pz}$ , area  $A_{pz}$ , mass  $m_{pz}$ , electro-mechanic coupling coefficient  $d_{33}$ , electrical capacitance  $C_p$ ;
- Passive supporting structure: Young modulus  $E_{stru}$ , area  $A_{stru}$ , bending stiffness  $I_{stru}$ .

**Table 9. Robustness analysis: study cases**

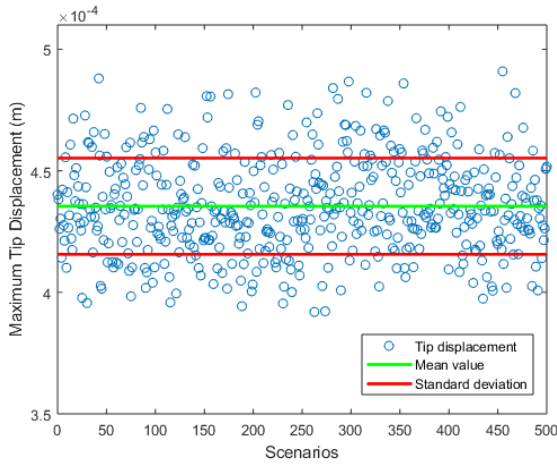
<b>Study Case 1</b>	10% uncertainty on piezo devices mechanical and electrical properties
<b>Study Case 2</b>	10% uncertainty on piezo and supporting structure mechanical and electrical properties
<b>Study Case 3</b>	20% uncertainty on piezo devices mechanical and electrical properties
<b>Study Case 4</b>	20% uncertainty on piezo and supporting structure mechanical and electrical properties



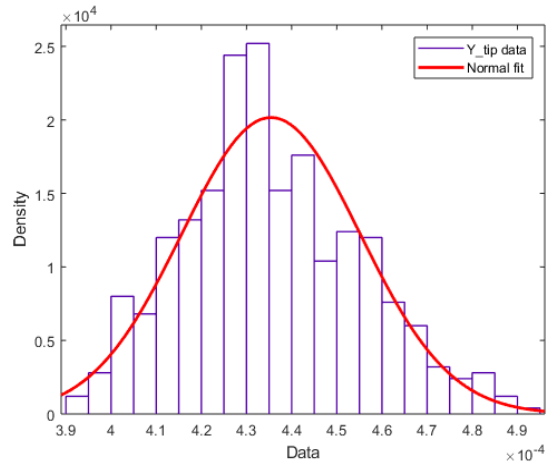
**Figure 26. Study Case 1 - Maximum tip displacement:**  $\mu = 4.3358e-04$ ,  $\sigma = 1.4823e-06$



**Figure 27. Study Case 1 - Normal distribution of tip displacement data set**

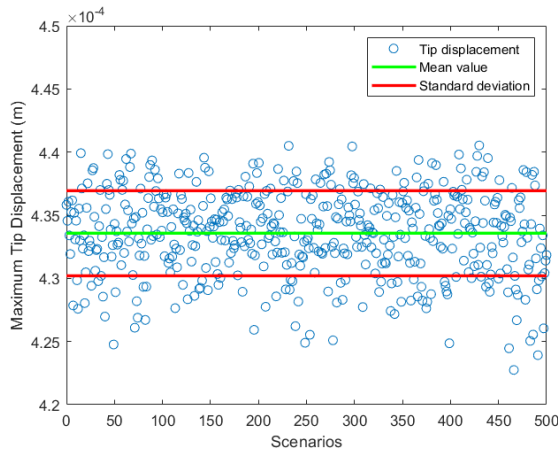


**Figure 28. Study Case 2 - Maximum tip displacement:**  $\mu = 4.3542e-04$ ,  $\sigma = 1.9784e-05$

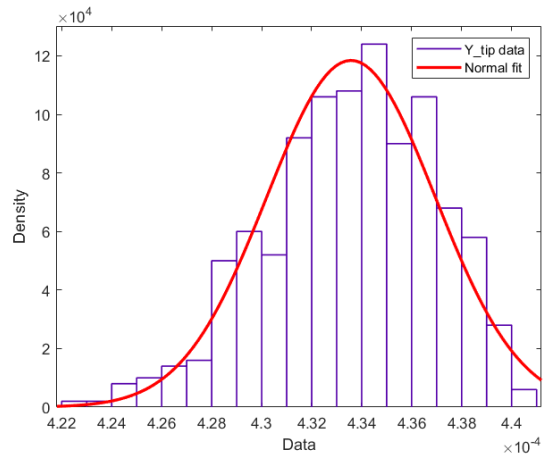


**Figure 29. Study Case 2 - Normal distribution of tip displacement data set**

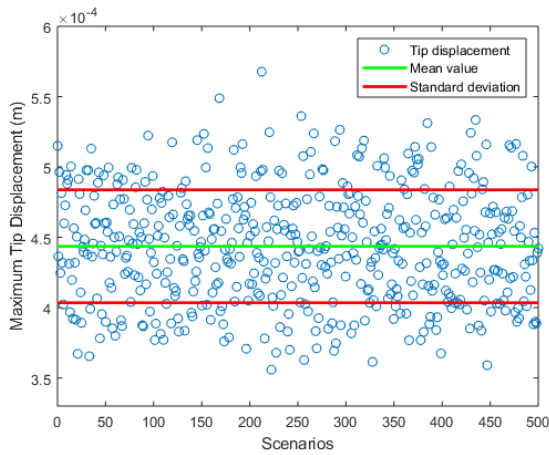
The controller robustness has been assessed by adding uncertainties to the aforementioned parameters. In Figure 26 to Figure 33 the maximum tip displacement and its normal fit are reported, along with the data mean value and standard deviation. As expected, the presence of uncertainties affecting piezo-electric actuators properties does not lead to excessive changes in the system response, thus in accordance with previous analyses about damaged devices. On the contrary, it is worth noting that, by introducing uncertainties on structural parameters, the mean value of the maximum tip displacement increases with respect to the cases in which only stack devices characteristics are uncertain. Furthermore, the standard deviation tends to grow by an order of magnitude.



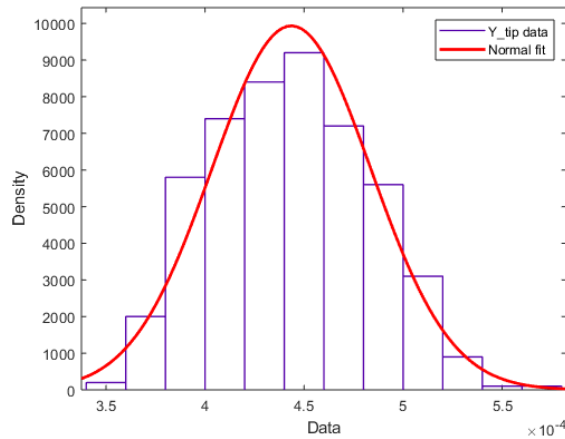
**Figure 30. Study Case 3 - Maximum tip displacement:  $\mu = 4.3357e-04$ ,  $\sigma = 3.3683e-06$**



**Figure 31. Study Case 3 - Normal distribution of tip displacement data set**



**Figure 32. Study Case 4 - Maximum tip displacement:  $\mu = 4.4358e-04$ ,  $\sigma = 4.0159e-05$**



**Figure 33. Study Case 4 - Normal distribution of tip displacement data set**

Nevertheless, such modifications does not represent a significant reduction of the damping capabilities of the active network, as demonstrated by the satisfactory narrow normal distributions associated to collected data.

## CONCLUSIONS

This paper aims at investigating the effects of uncertainties on the damping control system of a large space antenna supporting structure. The system equations of motion are derived accordingly to a classical Lagrangian formulation complemented with FEM theory. A network of active piezo-stack devices has been embedded into the passive supporting structure to counteract undesired disturbances originated by platform operations. The authority of each smart actuator is defined by the means of an optimization procedure: the optimal feedback gains distribution ensuring a minimum power consumption has been found and implemented. The dynamics of an orbiting satellite equipped with the truss-like supporting frame of a mesh reflector has been simulated, under orbital parameters selected to comply with real missions scenarios.

An integrated control system is proposed to damp the elastic vibrations induced on the flexible appendage by two attitude manoeuvres. The attitude re-orientation leading to the higher maximum tip displacement has been chosen for further analyses. By simulation analysis, the optimal gains identified by using a genetic algorithm demonstrated their effectiveness in damping unwanted elastic oscillations. The power to be supplied to the control system is affordable for a mesh reflector-equipped EO space mission.

In addition, the impact of a reduction of the actuators number is presented. The system was affected by such a decrease, thus leading to the conclusion that the more actuators are employed, the more vibrations are damped and the less power consumption is required. Furthermore, the robustness of the system to damages of the actuators has been explored. The damage has been simulated has a reduction of the 50% of the gain associated to randomly chosen actuators. Both by selecting a number  $N$  of randomly damaged piezo stacks and fixing  $N=40$ , the net demonstrated to guarantee a satisfactory damping capability.

Considering that space systems can vary their characteristics as a result of both launch campaign and in-orbit aging processes, a Monte Carlo simulations campaign has been carried out to evaluate the performance of the controller (which has been designed for the nominal case). Results have shown that the PD feedback controller is quite robust even to significant variations of both actuators and passive structure physical properties.

On account of this, it can be remarked that vibration damping by piezo stack actuators is a promising field of research for space antennas applications.

## REFERENCES

- <sup>1</sup> G.L. Ketner, "Survey of historical incidents with Control-Structures Interaction and recommended technology improvements needed to put hardware in space", prepared for *Control Structures Interaction Office, NASA, Langley Research Center*, Washington, 1989.
- <sup>2</sup> A. Falcoz, M. Watt, M. Yu, A. Kron et al., "Integrated Control and Structure Design framework for spacecraft applied to Biomass satellite", *Proceedings of the 19<sup>th</sup> IFAC Symposium on Automatic Control in Aerospace*, September 2-6, 2013, Wurzburg, Germany.
- <sup>3</sup> S. Benanni, F. Ankersen, M. Arcioni et al., "Robust Attitude Control Design for the BIOMASS Satellite (Earth Explorer Core Mission Candidate)", *Proceedings of the 18<sup>th</sup> IFAC Symposium on Automatic Control in Aerospace*, 28 August – 2 September, 2011, Milan, Italy.
- <sup>4</sup> Y. Luo et al., 'Active vibration control of a hoop truss structure with piezoelectric bending actuators based on a fuzzy logic algorithm', *Smart Mater. Struct.*, vol. 27, no. 8, p. 085030, 2018.
- <sup>5</sup> R. Xu, D. Li, J. Jiang, and J. Zou, 'Decentralized adaptive fuzzy vibration control of smart gossamer space structure', *J. Intell. Mater. Syst. Struct.*, vol. 28, no. 12, pp. 1670–1681, Jul. 2017.
- <sup>6</sup> Angeletti, Gasbarri, Sabatini, "Optimal Design of a Net of Adaptive Structures for Microvibration Control in Large Space Structures", *69<sup>th</sup> International Astronautical Congress*, IAC-18,C2,3,9,x43294, Brema, Germania, 1-5 Ottobre 2018.
- <sup>7</sup> P. Gasbarri, R. Monti, G. Campolo, and C. Toglia, 'Control-oriented modelization of a satellite with large flexible appendages and use of worst-case analysis to verify robustness to model uncertainties of attitude control', *Acta Astronautica*, vol. 81, no. 1, pp. 214–226, Dec. 2012
- <sup>8</sup> *Vibration Control of Active Structures: An Introduction*, A. Preumont, 3rd ed. Springer Netherlands, 2011
- <sup>9</sup> A. Pisculli and P. Gasbarri, 'A minimum state multibody/FEM approach for modeling flexible orbiting space systems', *Acta Astronautica*, vol. 110, pp. 324–340, May 2015.
- <sup>10</sup> V. Piefort, 'Finite Element Modelling of Piezoelectric Active Structures', Doctor of Applied Sciences, Université Libre de Bruxelles, Active Structures Laboratory Department of Mechanical Engineering and Robotics, 2001
- <sup>11</sup> F. di Scioscio, P. Gasbarri, C. Marianetti, and C. Toglia, 'Control of Vibrations of the International Space Station with Piezoelectric Actuators', in *Proceedings of the International Astronautical Federation*, Fukoka, Japan, 2005, vol. 6, pp. 16–21
- <sup>12</sup> N.R. Ravishankar et al., 'Reinforcement Learning Algorithms: Survey and Classification', in *Indian Journal of Science & Technology*, India, 2017, vol. 10, Issue 1